RSC Advances

PAPER

View Article Online
View Journal | View Issue

Cite this: *RSC Adv.*, 2025, **15**, 38036

A high-performance solar blind photodetector based on spinel gallium oxide thin film supported by aluminum doping

Yuehua An,[a] Wei Cui,[a] Jiangwei Liu,[a] Pengcheng Xu,[a] Zhensen Gao *[bc] and Weihua Tang*[d]

Metastable γ-phase gallium oxide (Ga_2O_3)-based semiconductor materials have recently garnered much attention for developing high-performance wide-band-gap optoelectronic devices. However, the difficulty in the synthesis of single-phase crystals and the poor thermal stability of metastable γ-Ga_2O_3 pose great obstacles for its potential applications. In this work, we experimentally demonstrate the epitaxial growth of γ-Ga_2O_3 thin films at 750 °C on α-Al_2O_3 (0001) substrates upon aluminum (Al) doping. A solar blind photodetector based on an Al-doped γ-Ga_2O_3 thin film was successfully fabricated, and its properties were investigated in detail. Benefiting from its high crystal quality and absence of oxygen vacancies in Al-doped γ-Ga_2O_3, the solar blind photodetector exhibited a very low dark current, fast decay time, high detectivity, and excellent wavelength selectivity, along with high stability and reproducibility. Notably, the present device exhibited no obvious performance degradation when the light intensity and bias voltage were increased, indicating good self-heating dissipation, which is beneficial for future practical applications. The γ-Ga_2O_3 thin film-based photodetector might open up new possibilities to obtain high-performance thin film-based solar blind ultraviolet optoelectronic devices.

Received 29th August 2025
Accepted 27th September 2025

DOI: 10.1039/d5ra06475a

rsc.li/rsc-advances

1. Introduction

Solar-blind ultraviolet (UV) detection with a cutoff wavelength shorter than 280 nm has a vast and growing number of military and civil surveillance applications, such as missile tracking, short-range secure communication, UV astronomy, ozone hole monitoring, and corona detection.[1–5] Commercial solar blind photodetectors (PDs) are mainly based on vacuum photomultiplier tubes, which have obvious disadvantages, such as high operation power consumption, inflexibility, and difficulty in integration, thereby limiting their practical applications.[6]

Recently, solar blind PDs based on wide-bandgap semiconductors, such as AlGaN, MgZnO, diamond, and Ga_2O_3, have attracted great attention.[7–10] However, high-quality epitaxial AlGaN films are difficult to be prepared due to their crystal deterioration with increasing Al content and the breakdown of the single wurtzite phase of MgZnO with increasing Mg content, and diamonds cannot be used to detect the entire solar-blind UV region because of their non-tunable bandgap.[10,11] Ga_2O_3 with a direct bandgap of 4.9–5.3 eV lies sharply in the solar-blind spectrum region and also exhibits a flexible tunability in bandgap by alloying with different materials, making it one of the ideal candidates to fabricate solar-blind UV PDs.[12–15] Ga_2O_3 is known to show five crystalline phases named α, β, γ, δ and ε.[16] Among these phases, the most stable monoclinic β-Ga_2O_3 has been widely studied. The solar-blind PDs based on Ga_2O_3 are concentrated on β-Ga_2O_3 because of its stability and ease of preparation. However, β-Ga_2O_3 has a monoclinic structure, which makes it difficult to grow high-quality β-Ga_2O_3 on hetero-substrates. It is challenging to find material lattices matching with the β-Ga_2O_3 lattice to grow epitaxial thin films for opto-electronic applications. Thus, it is meaningful to explore the potential application of other metastable materials with a hexagonal/cubic structure, which have the same structure as those of Al_2O_3, ZnO, SiC, GaN and $MgAl_2O_4$.[17–19] PDs based on other metastable phases have rarely been reported because of the difficulty in synthesizing single-phase crystals with thermal stability.

A recent first-principles study on the energetics of the Ga_2O_3 polymorphs suggests that the differences in free energy between the β-phase and other metastable phases are small; therefore, the polymorph of Ga_2O_3 is selected depending upon the preparation conditions.[20–22] Moreover, doping is an important

[a]*School of Optoelectronic Engineering, Guangdong Polytechnic Normal University, Guangzhou 510665, China*

[b]*Key Laboratory of Photonic Technology for Integrated Communication and Sensing, Ministry of Education, Guangdong University of Technology, Guangzhou 510006, China*

[c]*Guangdong Provincial Key Laboratory of Photonics Information Technology, Advanced Institute of Photonics Technology, School of Information Engineering, Guangdong University of Technology, Guangzhou 510006, China. E-mail: gaozhensen@gdut.edu.cn*

[d]*Innovation Center for Gallium Oxide Semiconductor (IC-GAO), College of Integrated Circuit Science and Engineering, Nanjing University of Posts and Telecommunications, Nanjing 210023, China. E-mail: whtang@njupt.edu.cn*

method to stabilize the crystal structure against thermal processes, making it a possible approach to obtain Ga_2O_3 with a thermally stabilized metastable phase and preventing the transition to the β-phase.[23–25] Acting as a satisfying high-quality Ga_2O_3 on hetero-substrates for developing high-performance wide-band-gap optoelectronic devices, metastable γ-phase Ga_2O_3 is considered here. Hiroyuki *et al.* have demonstrated the fabrication of Mn-doped γ-Ga_2O_3 at a temperature of 500 °C on α-Al_2O_3 (0001) substrates using the PLD method, which differs from the undoped film that shows the β phase.[26] Sam-Dong *et al.* have shown the enhancement of thermal stability of α-Ga_2O_3 films on sapphire substrates upon Al doping. The films can be grown at a temperature as high as 800 °C and can withstand an annealing temperature as high as 850 °C without forming the β phase.[23] Furthermore, Yue *et al.* have reported the synthesis of metastable γ-Ga_2O_3 nanoflowers with hexagonal nanopetals by the oxidation of metallic Ga in solutions.[27] The γ-Ga_2O_3 nanoflowers show excellent solar-blind detection performance; however, the poor thermal stability of the metastable phase still hinders the target application. Until now, the difficulty in synthesizing single-phase crystals and the poor thermal stability of the metastable γ-phase of Ga_2O_3 have greatly limited its potential applications in wide-band-gap high-performance optoelectronic devices.

In this work, the Al-doped γ-Ga_2O_3 thin film was epitaxially grown on α-Al_2O_3 (0001) substrates using the radio frequency magnetron sputtering technique, with the growth temperature successfully increased to 750 °C. A solar blind PD based on Al-doped γ-Ga_2O_3 thin film was successfully constructed. The PD shows excellent photoelectric properties. The γ-Ga_2O_3 thin film-based PDs might open up new possibilities for obtaining high-performance thin film-based solar blind UV optoelectronic devices.

2. Experimental section

2.1. Preparation and characterization of Ga_2O_3 thin films

The film samples were prepared on top of (0001) oriented single-crystal α-Al_2O_3 substrates using radio frequency (RF) magnetron sputtering. The Ga_2O_3 ceramic ($\pi \times 30^2 \times 8$ mm^3, 99.99% purity) with/without embedded Al_2O_3 ceramic ($\pi \times 12.5^2 \times 4$ mm^3, 99.99% purity) was used as a target for Al-doped/pure Ga_2O_3 thin film preparations, respectively. In the experiment, the Al_2O_3 target was covered at the glow circle position of the Ga_2O_3 target, and the incorporation amount was fine-tuned by varying the size of the coverage area. The base pressure in the chamber was 1×10^{-4} Pa, and the distance between the Ga_2O_3 target and the substrate was 6 cm. The flow rate of Ar (99.999% purity) gas was fixed to 24 sccm by a mass flow controller. The films were deposited at a working pressure of 1 Pa and RF power of 70 W for 2 h. The substrate temperature was fixed at 750 °C. The crystal structures of the as-grown films were investigated by a PANalytical X'pert PRO diffractometer using Cu Kα ($\lambda = 1.5405$ Å) radiation. The structural quality was estimated by X-ray rocking curve (XRC) measurements using Smart Lab X-ray diffraction (XRD). The surface morphologies were characterized by a Hitachi S-4800 field emission scanning electron microscope (FE-SEM). UV-visible (UV-vis) absorption spectra were taken using a Hitachi U-3900 UV-vis spectrophotometer. The elemental content was analyzed using X-ray photoelectron spectroscopy (XPS).

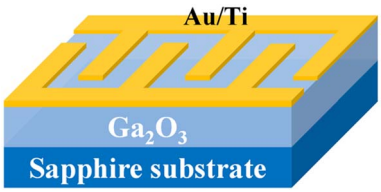

Fig. 1 Schematic of an MSM structure PD.

2.2. Fabrication and characterization of the photodetector

To construct a metal–semiconductor-metal (MSM) PD, a three-pair interdigital Au/Ti electrode was deposited on the film by RF magnetron sputtering, as illustrated in Fig. 1. The Au/Ti electrode is chosen because the affinity of Ga_2O_3 is close to the work function of Ti, making it easy to form ohmic contact. The width and length of the electrode fingers were 200 μm and 2800 μm, respectively. The spacing gap was 200 μm. A small point electrode (~0.1 mm diameter) of indium metal was also pressed onto the Au/Ti electrode as connection points with a Cu wire. A Keithley 2450 source meter was utilized to measure the current–voltage (*I–V*) and time-dependent photoresponse of the Ga_2O_3 film-based PD. A UV lamp (~7 W) with wavelengths of 254 nm and 365 nm was used as the light source, and the light irradiation power density was tuned by adjusting the distance between the light source and the sample.

3. Results and discussion

The XRD patterns of undoped and Al-doped Ga_2O_3 thin films are shown in Fig. 2(a). The undoped Ga_2O_3 thin film formed on the α-Al_2O_3 substrate is a monoclinic β phase, as determined by XRD (JCPDS Card No. 43-1012). Besides the diffraction peaks of the Al_2O_3 substrate, diffraction peaks located at around 18.88°, 38.17°, and 58.88° are observed for the undoped film, which corresponds well to the β ($\bar{2}01$), β ($\bar{4}02$) and β ($\bar{6}03$) lattice planes, respectively. The Al-doped Ga_2O_3 thin film formed on the α-Al_2O_3 substrate is a cubic γ phase, as determined by XRD (JCPDS Card No. 20-0426). Besides the diffraction peaks of the Al_2O_3 substrate, diffraction peaks located at around 18.67°, 37.85°, and 58.49° are observed for the Al-doped film, which corresponds well to the γ (111), γ (222) and γ (333) lattice planes, respectively. The X-ray rocking curves of γ-Ga_2O_3 (111) and β-Ga_2O_3 ($\bar{2}01$) planes are shown in Fig. 2(b) and (c) for the Al-doped and undoped films, respectively, and correspond to the FWHM values of 3672 and 5184 arcsec. The result indicates that the crystal quality of the as-grown γ-Ga_2O_3 film is better than that of the β-Ga_2O_3 film, the preparation conditions of which are similar.

The top-view SEM morphologies of the Al-doped γ-Ga_2O_3 film and undoped β-Ga_2O_3 film are presented in Fig. 3(a). It is obvious that the γ-Ga_2O_3 and β-Ga_2O_3 films appear to form

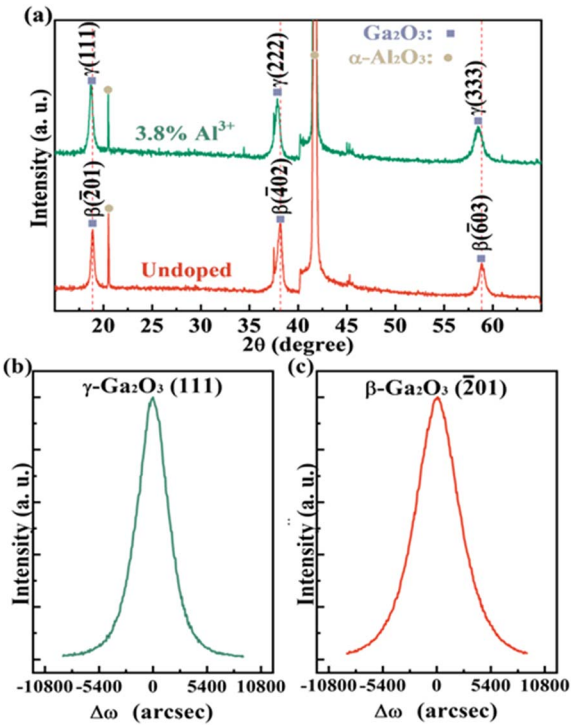

Fig. 2 (a) XRD patterns of undoped and Al-doped Ga_2O_3 films. X-ray rocking curves of (b) γ-Ga_2O_3 (111) for the Al-doped film and (c) β-Ga_2O_3 ($\bar{2}$01)for the undoped film.

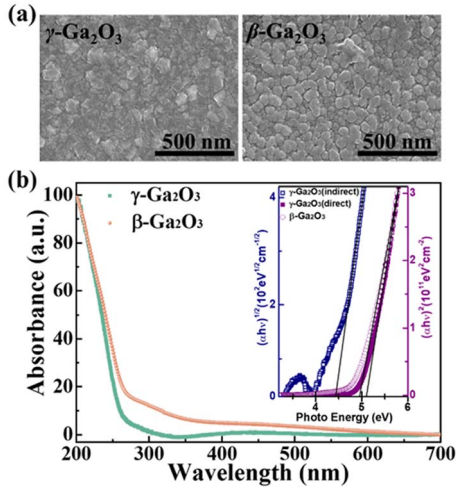

Fig. 3 (a) SEM images of the Al-doped γ-Ga_2O_3 and undoped β-Ga_2O_3 films. (b) UV-vis absorbance spectra of the Al-doped γ-Ga_2O_3 and undoped β-Ga_2O_3 films with the plot of $(\alpha h\nu)^2$ and $(\alpha h\nu)^{1/2}$ *vs.* $h\nu$ in the inset.

different surface structures on (0001) sapphire substrates. For the γ-Ga_2O_3 film, irregular pseudo-pyramid structures are distributed randomly on the surface, and the grain boundary is not clear; a similar surface structure has been observed for cubic-In_2O_3 on (0001) sapphire substrates in our previous study.[28] The surface structures of the β-Ga_2O_3 film are columnar-like, and a clear grain boundary can be observed. Fig. 3(b) shows the UV-vis absorbance spectrum of the Al-doped γ-Ga_2O_3 film and the undoped β-Ga_2O_3 film. It is evident that all the films have significant absorption edges at ~250 nm, near the lower edge of the solar-blind region. Moreover, the bandgap of the semiconductor film can be evaluated by extrapolating the linear region of the plots of $(\alpha h\nu)^2$ and $(\alpha h\nu)^{1/2}$ *versus* $h\nu$ for direct and indirect transitions, respectively. For β-phase Ga_2O_3, a direct bandgap semiconductor, the bandgap value was determined to be 4.94 eV, as shown in the inset of Fig. 3(b). As the transition type of γ-phase Ga_2O_3 is undefined, both the direct and indirect bandgaps were estimated for the Al-doped γ-Ga_2O_3 film. The direct and indirect bandgap values were determined to be 5.08 and 4.43 eV, respectively, which were slightly higher than those for undoped γ-Ga_2O_3 (5.0 and 4.4 eV, respectively).[19]

XPS analysis was performed to elucidate the chemical compositions and oxygen deficiency in the as-grown films. The surface of the films was etched by Ar^+ bombardment before the XPS measurement. Fig. 4(a) shows the wide survey spectrum in the binding energy range from −40 eV to 1350 eV to identify the elements in the Al-doped γ-Ga_2O_3 film. XPS peaks of Ga, O, Al and C were indicated in the Figure, and there were no other elements detected from the wide survey spectrum of the film. The charge-shift spectrum was calibrated using the C 1s peak at 284.8 eV. The Al 2p core level peak of the Al-doped γ-Ga_2O_3 film is presented in Fig. 4(b), and the energy peak center is observed at 71.1 eV. The peak position shows a significant shift compared to the Al 2p peak in pure Al_2O_3 film on the same substrate (74.5 eV). A similar phenomenon was also observed with a negative shift for the Al 2p peak during the formation of Al–O–Ga bonds.[14] In their report, the peak position was noted at 73.9 eV in the $(Al_{0.22}Ga_{0.78})_2O_3$ film; the significant shift in our result indicates that Al is present in the Al-doped γ-Ga_2O_3 film in the form of Al–O–Ga bonds. We have not yet identified whether the Al–O–Ga bonds are the key factors to obtain stabilized γ-Ga_2O_3, but they are a very significant sign to understand if the growing film is in the γ phase or not. The Ga 3d core level peaks of the Al-doped γ-Ga_2O_3 and undoped β-Ga_2O_3 films are shown in Fig. 4(c), with the energy peak centers observed at 19.7 eV and 20.1 eV, respectively. The O 1s core level peaks of the Al-doped γ-Ga_2O_3 and undoped β-Ga_2O_3 films are shown in Fig. 4(d), and the energy peaks are observed at 530.2 eV and 530.6 eV, respectively. The O 1s peaks can be divided into two components: I and II; peak I is attributed to lattice oxygen ions, and peak II is attributed to the oxygen ions in the oxygen vacancy region and surface defects of the film.[5,10] The intensity of oxygen vacancies and surface defects in the film has a significant negative influence on the performance of Ga_2O_3 thin film-based PDs, such as dark current and response speed.[29] The peak ratios of II/I were 1/5 and 1/3 for Al-doped γ-Ga_2O_3 and pure β-Ga_2O_3, respectively [Fig. 4(d)], which indicates a lower intensity of oxygen vacancies and surface defects in the Al-doped γ-Ga_2O_3 film than in the pure β-Ga_2O_3 film.

Fig. 5 shows the room-temperature *I–V* characteristics of the PD based on an Al-doped γ-Ga_2O_3 thin film in the dark, under 365 nm (100 μW cm^{-2}) and 254 nm (with various light intensities) light illumination. The *I–V* curve in the dark is linear,

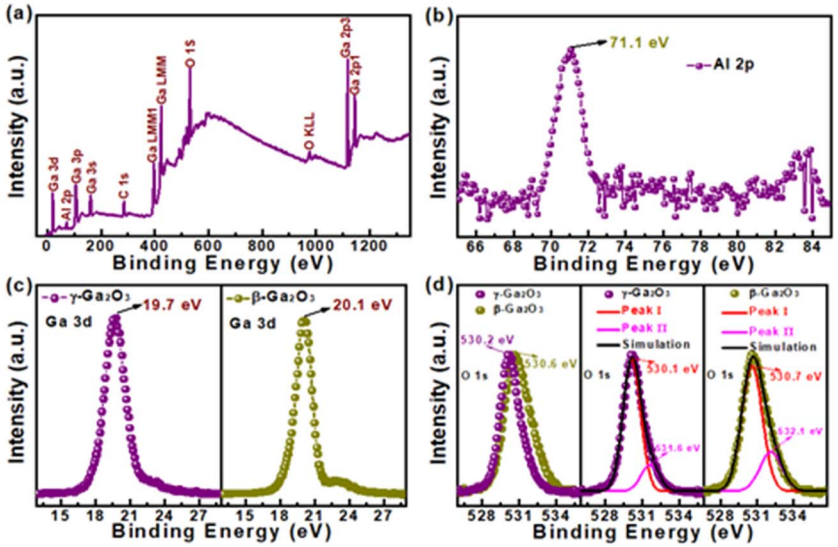

Fig. 4 (a) XPS wide survey spectrum and (b) core level of Al 2p for the Al-doped γ-Ga_2O_3 film. Core levels of (c) Ga 3d and (d) O 1s for Al-doped γ-Ga_2O_3 and undoped β-Ga_2O_3 films.

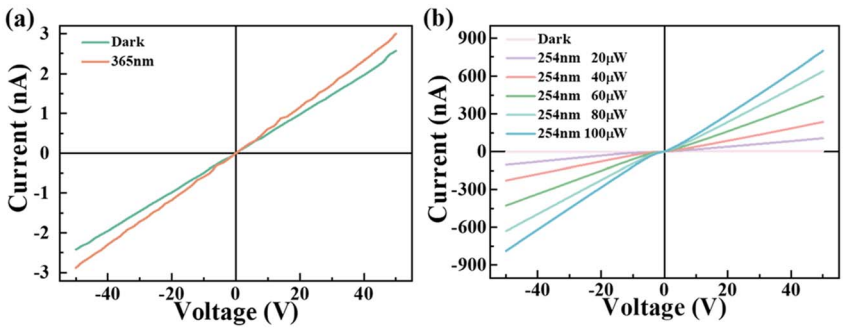

Fig. 5 (a) *I–V* characteristics of the Al-doped γ-Ga_2O_3 thin film-based MSM structure PD in the dark and under a 365 nm light illumination. (b) *I–V* characteristics of the device in the dark and under a 254 nm light illumination with various light intensities.

indicating that the contact is of an ohmic type. The corresponding resistance is 19.5 GΩ, and the dark current is about 2.57 nA at a voltage of 50 V, as shown in Fig. 5(a), which is much lower than that of undoped β-Ga_2O_3 films (about 100 nA at a voltage of 10 V), as per our previous reports. The *I–V* curve under 365 nm light illumination indicates that the device is almost insensitive to 365 nm light illumination, as shown in Fig. 5(a). Meanwhile, the device has significant sensitivity for 254 nm light illumination, as shown in Fig. 5(b).

In order to further investigate the performance of the Al-doped γ-Ga_2O_3 thin film-based PD, the time-dependent photoresponse to solar-blind UV illuminations was investigated, as shown in Fig. 6. Fig. 6(a) and (b) show the time-dependent photoresponse of the device to 254 nm UV light illuminations with varied light intensities and bias voltages, respectively. The device shows excellent photoelectric performance, with the photocurrent gradually increasing with increasing incident light intensities and bias voltages. The larger the voltage applied, the higher the I_{photo} obtained, following the basic photoconductance rule, which works as a photo-sensitive resistance. The higher the light intensity, the higher the I_{photo} output, as more photo-generated carriers would be devoted to I_{photo} at a certain voltage. Another important performance parameter of solar blind PDs is the response time. To study the response time of the device, the current rising and decaying process can be derived by fitting the photoresponse curve with the following relaxation equation:[30]

$$I = I_0 + Ae^{-t/\tau_1} + Be^{-t/\tau_2} \quad (1)$$

where I_0 is the photocurrent in the steady state, A and B are the constant values, t is the time, and τ_1 and τ_2 are the relaxation time constants. As shown in Fig. 6(c) and (d), the photoresponse processes fit quite well. We note that the rising edge consists of two components (τ_{r1} and τ_{r2}), and the decaying edge is steep, consisting of only one component. It has been estimated that the rise edge constants τ_{r1} and τ_{r2} are around 2.39 s/12.57 s, 1.52 s/8.16 s, 1.02 s/6.92 s and 0.88 s/5.89 s for the device under 20 μW cm^{-2}, 40 μW cm^{-2}, 60 μW cm^{-2} and 80 μW cm^{-2} light illuminations at a bias voltage of 50 V, respectively. In contrast, the rise edge constants τ_{r1} and τ_{r2} are estimated to be 1.22 s/

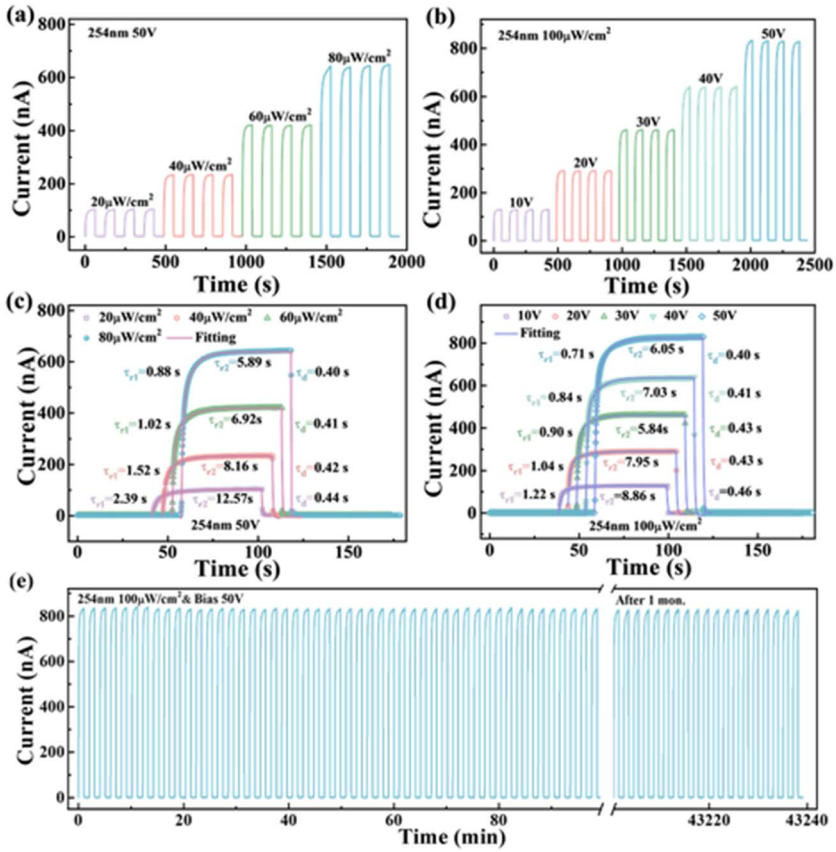

Fig. 6 Time-dependent photoresponse of the Al-doped γ-Ga_2O_3 thin film-based MSM structure PD measured under different conditions: (a) photoresponse of the device under different light intensities at 50 V; (b) photoresponse of the device at different bias voltages under 100 μW cm^2; (c) experimental curve and fitted curve of the current rising and decaying process of the device under different light intensities at 50 V; (d) experimental curve and fitted curve of the current rising and decaying process of the device at different bias voltages under 100 μW cm^2; (e) photoresponse stability of the device during a long time test and after storage for one month.

8.86 s, 1.04 s/7.95 s, 0.90 s/5.84 s, 0.84 s/7.03 s and 0.71 s/6.05 s for the device under 100 μW cm^{-2} light illuminations at bias voltages of 10 V, 20 V, 30 V, 40 V and 50 V, respectively. It is obvious that the rise speed increases with both light intensity and bias voltage. Generally, the fast-response component can be attributed to the rapid change in carrier concentration that occurs as soon as the light is turned on or off, while the slow-response component is caused by carrier trapping/releasing owing to the existence of oxygen vacancies and other surface defects in the Al-doped γ-Ga_2O_3 film. It is evident that, when there are plenty of photon-generated carriers under stronger intensities of light illumination, the trapping/releasing effect is easier to saturate, so the response time is shorter; when the applied bias voltage is higher, the photo-generated electrons and holes undergo a rapid separation and then transfer toward the corresponding electrodes, resulting in a faster response speed. The decay edge constants τ_d are estimated to be 0.44 s, 0.42 s, 0.41 s and 0.40 s for the device under 20 μW cm^{-2}, 40 μW cm^{-2}, 60 μW cm^{-2} and 80 μW cm^{-2} light illuminations at a bias voltage of 50 V, respectively. The decay edge constants τ_d are estimated to be 0.46 s, 0.43 s, 0.43 s, 0.41 s and 0.40 s for the device under 100 μW cm^{-2} light illumination at bias voltages of 10 V, 20 V, 30 V, 40 V and 50 V, respectively. Due to the absence of oxygen vacancies in Al doped γ-Ga_2O_3 film, the trapping/releasing effect is a localization transport process without plentiful of photon-generated carriers when the light is off. It can hardly influence the photoconductance of the device, so the decaying edge is quite steep.

To quantitatively assess the device performance of the present solar blind photodetector, both responsivity (R_λ) and detectivity (D^*) were calculated, as shown in Fig. 7(a) and (c) as a function of light intensity and bias voltage, respectively. R_λ, which is defined as the photocurrent generated per unit power of incident light on the effective area of a PD, is calculated by the following equation:[2]

$$R_\lambda = (I_{light} - I_{dark})/(P_\lambda \cdot S) \quad (2)$$

where I_{light} is the light current, I_{dark} is the dark current of the device when illuminated with a light source, P_λ is the light intensity illuminated on the device, S is the effective illuminated area ($S = 3.24$ mm^2), and λ is the wavelength of the illuminating light.

Detectivity, which is usually used to evaluate the smallest detectable of a PD, can be calculated as follows:[31]

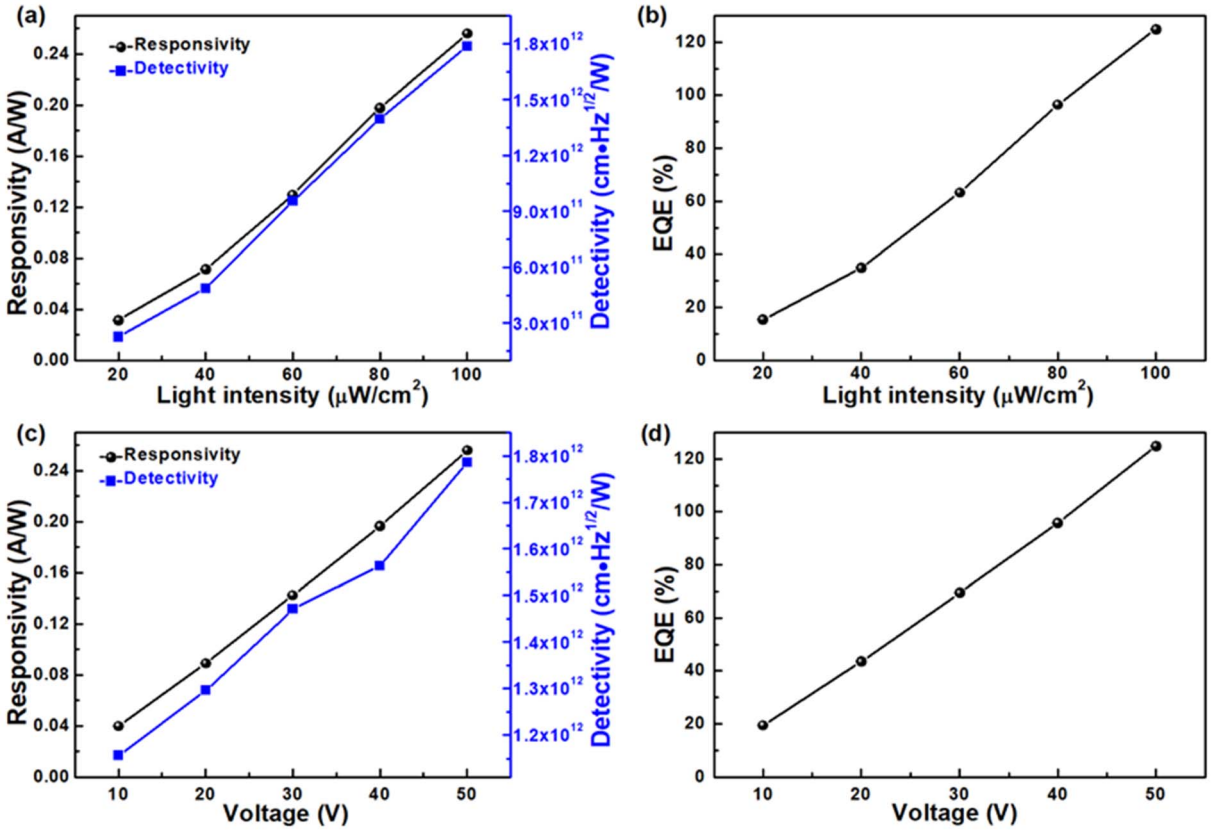

Fig. 7 (a) Responsivity and detectivity of the Al-doped γ-Ga_2O_3 thin film-based MSM structure PD as a function of bias voltage. (b) External quantum efficiency of the device as a function of bias voltage. (c) Responsivity and detectivity of the device as a function of light intensity. (d) External quantum efficiency of the device as a function of light intensity.

$$D^* = \frac{R_\lambda A^{1/2}}{(2eI_{\text{dark}})^{1/2}} \quad (3)$$

where R_λ is the responsivity, A is the effective area of the present device channel ($A = 3.24$ mm^2), e is the electronic charge, and I_{dark} is the dark current. It is clear that both the R_λ and D^* values increase with increasing light intensity and bias voltage. Specifically, the responsivity and detectivity are as high as 0.26 A W^{-1} and 1.79×10^{12} under 100 μW cm^{-2} light illumination at 50 V, respectively. Notably, the present device exhibits no obvious performance degradation with increasing light intensity and bias voltage, indicating that the device has good self-heating dissipation. Moreover, the external quantum efficiency (EQE) is also the key parameter to evaluate the performance of a PD, which is defined as the number of electrons probed per incident photon and can be calculated as follows:[32]

$$\text{EQE} = \frac{hcR_\lambda}{e\lambda} \quad (4)$$

where R_λ is the responsivity, h is Planck's constant, c is the velocity of light, e is the electronic charge, and λ is the exciting wavelength of the solar blind light. The EQE gradually increases with increasing light intensity and bias voltage, reaching a maximum of 124.92% under 100 μW cm^{-2} light illumination at 50 V, as shown in Fig. 7(b) and (d).

In order to investigate the spectral selectivity of the present device, the spectral responsivity was measured in the range of 225 to 600 nm, as shown in Fig. 8. It can be observed that the device shows excellent wavelength selectivity: it has highest responsivity at a wavelength of about 230 nm; as the wavelength increases, the responsivity gradually decreases and reaches

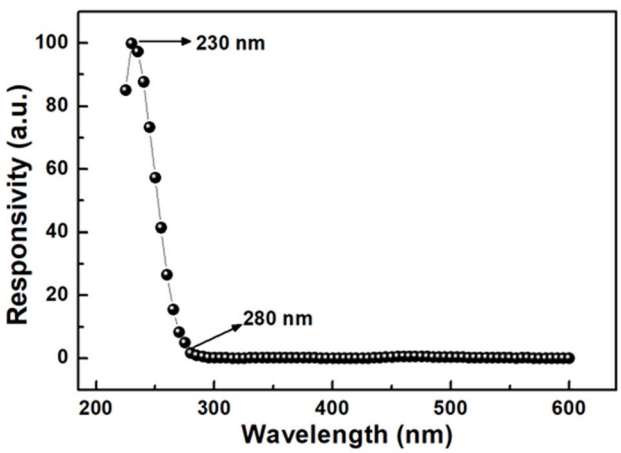

Fig. 8 Normalized spectral selectivity of the Al-doped γ-Ga_2O_3 thin film-based MSM structure PD.

a minimum value at about 280 nm. The rejection ratio of responsivity values for the solar blind region *versus* the solar visible region was estimated by dividing the responsivity at 230 nm by that at 280 nm. The excellent rejection ratio was evaluated at 60.98, indicating an excellent solar-blind UV response. The higher rejection ratio can be attributed to the better crystal quality and the absence of oxygen vacancies in Al-doped γ-Ga_2O_3.[33]

4. Conclusion

The Al-doped γ-Ga_2O_3 thin film was epitaxially grown on α-Al_2O_3 (0001) substrates by radio frequency magnetron sputtering, and the growth temperature was successfully increased to 750 °C. The solar blind UV PD based on the as-grown thin film exhibits excellent solar-blind UV photoelectric properties. Under 100 μW cm^{-2} 254 nm light illumination at a bias voltage of 50 V, the device exhibits a rise and decay time of 0.71 s/6.05 s and 0.40 s, responsivity of 0.26 A W^{-1}, detectivity of 1.79×10^{12}, and an EQE of 124.92%, along with high stability and reproducibility. Remarkably, the present device exhibits no obvious performance degradation with increasing light intensity and bias voltage. It indicates that the device has good self-heating dissipation, which will be beneficial for future practical applications. Moreover, the device shows excellent wavelength selectivity with a solar blind/visible rejection ratio of 60.98, which is nearly blind to photons with wavelengths longer than 280 nm. These results suggest that γ-Ga_2O_3 thin film-based PDs can open up new possibilities for obtaining high performance thin film-based solar blind UV optoelectronic devices.

Conflicts of interest

There are no conflicts of interest to declare.

Data availability

The data supporting this article are available from the corresponding author upon reasonable request.

Acknowledgements

National Key R&D Program of China (2023YFB2906000); National Natural Science Foundation of China (62375055); Guangdong Basic and Applied Basic Research Foundation (2023B1515020088); Basic and Applied Basic Research Project of Guangzhou Basic Research Program (2025A04J5417) and the Start-Up Funding of Guangdong Polytechnic Normal University (2022SDKYA013) are greatly acknowledged.

References

1 Y. Zhao, J. Zhang, D. Jiang, *et al.*, Ultraviolet photodetector based on a MgZnO film grown by radio-frequency magnetron sputtering, *ACS Appl. Mater. Interfaces*, 2009, **1**(11), 2428–2430.
2 W. Cui, D. Y. Guo, X. L. Zhao, *et al.*, Solar-blind photodetector based on Ga_2O_3 nanowires array film growth from inserted Al_2O_3 ultrathin interlayers for improving responsivity, *RSC Adv.*, 2016, **6**(103), 100683–100689.
3 Z. Li, T. Yan and X. Fang, Low-dimensional wide-bandgap semiconductors for UV photodetectors, *Nat. Rev. Mater.*, 2023, **8**(9), 587–603.
4 X. Zhu, Y. Wu, Z. Pan, *et al.*, Advancements in Ga_2O_3-based heterojunction ultraviolet photodetectors: Types, fabrication techniques, and integrated materials for enhancing photoelectric conversion efficiency, *J. Alloys Compd.*, 2025, **1010**, 177757.
5 Y. H. An, Z. S. Gao, Y. Guo, *et al.*, One ε-Ga_2O_3-based solar-blind Schottky photodetector emphasizing high photocurrent gain and photocurrent-intensity linearity, *Chin. Phys. B*, 2023, **32**(5), 058502.
6 Y. Li, T. Tokizono, M. Liao, *et al.*, Efficient Assembly of Bridged β-Ga_2O_3 Nanowires for Solar-Blind Photodetection, *ACS Appl. Mater. Interfaces*, 2010, **20**(22), 3972–3978.
7 Y. Gao, J. Yang, X. Ji, *et al.*, Semipolar (1122) AlGaN-based solar-blind ultraviolet photodetectors with fast response, *ACS Appl. Mater. Interfaces*, 2022, **14**(18), 21232–21241.
8 M. M. Fan, K. W. Liu, X. Chen, *et al.*, Mechanism of Excellent Photoelectric Characteristics in Mixed-Phase ZnMgO Ultraviolet Photodetectors with Single Cutoff Wavelength, *ACS Appl. Mater. Interfaces*, 2015, **7**(37), 20600–20606.
9 J. Ye, S. Jin and Y. Cheng, Photocurrent ambipolar behavior in phase junction of a Ga_2O_3 porous nanostructure for solar-blind light control logic devices, *ACS Appl. Mater. Interfaces*, 2024, **16**(20), 26512–26520.
10 R. Jin, J. Liu, S. Chen, *et al.*, Ultrasensitive Self-Powered Flexible Crystalline β-Ga_2O_3-Based Photodetector Obtained through Lattice Symmetry and Band Alignment Engineering, *ACS Appl. Mater. Interfaces*, 2024, **16**(32), 42406–42414.
11 T. Oshima, T. Okuno and S. Fujita, Ga_2O_3 Thin Film Growth onc-Plane Sapphire Substrates by Molecular Beam Epitaxy for Deep-Ultraviolet Photodetectors, *Jpn. J. Appl. Phys.*, 2007, **46**(11R), 7217–7220.
12 Z. Y. Wang, G. Zhang, X. J. Zhang, *et al.*, Polarization-sensitive artificial optoelectronic synapse based on anisotropic β-Ga_2O_3 single crystal for neuromorphic vision systems and information encryption, *Adv. Opt. Mater.*, 2024, **12**(29), 2401256.
13 T. Oshima, Y. Kato, M. Oda, *et al.*, Epitaxial growth of gamma-$(Al_xGa_{1-x})O_3$ alloy films for band-gap engineering, *Appl. Phys. Express*, 2017, **10**(5), 051104.
14 H. Xu, Y. Weng, K. Chen, *et al.*, Ultra-low BER encrypted communication based on self-powered bipolar photoresponse ultraviolet photodetector, *Adv. Opt. Mater.*, 2024, **10**, 2402238.
15 P. Li, L. Dong, C. Li, *et al.*, Indium doping-assisted monolayer Ga_2O_3 exfoliation for performance-enhanced MOSFETs, *Nanoscale*, 2023, **15**(28), 12105–12115.
16 R. Roy, V. Hill and E. Osborn, Polymorphism of Ga_2O_3 and the System Ga_2O_3-H_2O, *J. Am. Chem. Soc.*, 1952, **74**(3), 719–722.

17 X. C. Xia, Y. P. Chen, Q. J. Feng, *et al.*, Hexagonal phase-pure wide band gap epsilon-Ga_2O_3 films grown on 6H-SiC substrates by metal organic chemical vapor deposition, *Appl. Phys. Lett.*, 2016, **108**(20), 202103.
18 S. Fujita, M. Oda, K. Kaneko, *et al.*, Evolution of corundum-structured III-oxide semiconductors: Growth, properties, and devices, *Jpn. J. Appl. Phys.*, 2016, **55**(12), 1202A3.
19 T. Oshima, T. Nakazono, A. Mukai, *et al.*, Epitaxial growth of gamma-Ga_2O_3 films by mist chemical vapor deposition, *J. Cryst. Growth*, 2012, **359**(15), 60–63.
20 S. Yoshioka, H. Hayashi, A. Kuwabara, *et al.*, Structures and energetics of Ga_2O_3 polymorphs, *J. Phys.: Condens. Matter*, 2007, **19**(34), 346211.
21 H. Nishinaka, D. Tahara and M. Yoshimoto, Heteroepitaxial growth of epsilon-Ga_2O_3 thin films on cubic (111) MgO and (111) yttria-stablized zirconia substrates by mist chemical vapor deposition, *Jpn. J. Appl. Phys.*, 2016, **55**(12), 1202BC.
22 S. X. Ge and Z. Zheng, Phase controllable synthesis of unusual epsilon-Ga_2O_3 single crystals with promising luminescence property, *Solid State Sci.*, 2009, **11**(9), 1592–1596.
23 S. D. Lee, Y. Ito, K. Kaneko, *et al.*, Enhanced thermal stability of alpha gallium oxide films supported by aluminum doping, *Jpn. J. Appl. Phys.*, 2015, **54**(3), 030301.
24 R. Lorenzi, N. V. Golubev, E. S. Ignat'eva, *et al.*, Defect-assisted photocatalytic activity of glass-embedded gallium oxide nanocrystals, *J. Colloid Interface Sci.*, 2022, **608**(3), 2830–2838.
25 G. Yang, H. A. Ni, H. D. Liu, *et al.*, The doping effect on the crystal structure and electrochemical properties of $LiMn_xM_{1-x}PO_4$ (M = Mg, V, Fe, Co, Gd), *J. Power Sources*, 2011, **196**(10), 4747–4755.
26 H. Hayashi, R. Huang, H. Ikeno, *et al.*, Room temperature ferromagnetism in Mn-doped gamma-Ga_2O_3 with spinel structure, *Appl. Phys. Lett.*, 2006, **89**(18), 181903.
27 Y. Teng, L. X. Song, A. Ponchel, *et al.*, Self-Assembled Metastable gamma-Ga_2O_3 Nanofl owers with Hexagonal Nanopetals for Solar-Blind Photodetection, *Adv. Mater.*, 2014, **26**(36), 6238–6243.
28 W. Cui, X. L. Zhao, Y. H. An, *et al.*, Direct charge carrier injection into Ga_2O_3 thin films using an In_2O_3 cathode buffer layer: their optical, electrical and surface state properties, *J. Phys. D Appl. Phys.*, 2017, **50**(13), 135109.
29 D. Guo, P. Li, Z. Wu, *et al.*, Inhibition of unintentional extra carriers by Mn valence change for high insulating devices, *Sci. Rep.*, 2016, **6**(1), 24190.
30 D. Y. Guo, Z. P. Wu, P. G. Li, *et al.*, Fabrication of beta-Ga_2O_3 thin films and solar-blind photodetectors by laser MBE technology, *Opt. Mater. Express*, 2014, **4**(5), 1067–1076.
31 W. Y. Kong, G. A. Wu, K. Y. Wang, *et al.*, Graphene-beta-Ga_2O_3 Heterojunction for Highly Sensitive Deep UV Photodetector Application, *Adv. Mater.*, 2016, **28**(48), 10725.
32 J. M. Wu and W. E. Chang, Ultrahigh Responsivity and External Quantum Efficiency of an Ultraviolet-Light Photodetector Based on a Single VO_2 Microwire, *ACS Appl. Mater. Interfaces*, 2014, **6**(16), 14286–14292.
33 A. S. Pratiyush, S. Krishnamoorthy, S. V. Solanke, *et al.*, High responsivity in molecular beam epitaxy grown beta-Ga_2O_3 metal semiconductor metal solar blind deep-UV photodetector, *Appl. Phys. Lett.*, 2017, **110**(22), 221107.